Blind Image Deblurring using GLCM and ElasticNet Regularization

JOTHI LAKSHMI S[A], DEEPA P[B], RAMESH KUMAR M [C], MOHANRAJ A[D]

[a] *Associate Professor, Department of CSE, Akshaya college Engineering and technology, Coimbatore, TamilNadu, India,*

[b] *Associate Professor, Department of ECE, Government college of technology, Coimbatore, TamilNadu, India,*

[c] *Professor, Department of IT, VSB College of Engineering Technical Campus, Coimbatore, TamilNadu, India,*

[d] *Assistant Professor, Department of CSE, Sri Eshwar college of Engineering, Coimbatore, TamilNadu, India,*

ABSTRACT

The well-known source of digital degradation is camera shake, photos under dim light and a handheld camera etc. Extensive research has taken place over the last decade in the field of retrieving a latent image from burry input; most of them work quite well, but very often incur to blur in edges. This paper has been proposed a new deblurring method in which the high-frequency layer is extracted from the blurred image using a 2D Haar wavelet transform in the luminance channel, then from the high-frequency layer, rich edge region is extracted using GLCM and sliding window concepts after the canny edge detection process. Finally, the extracted rich edge region is used to estimate the blur kernel using the elastic net regularization of singular value. Here regularization is used to avoid over-fitting of the data and reduces the blurring effects of the image. Experimental result demonstrates that the proposed deblurring algorithm achieves the better results on natural images which are evaluated using the parameter such as PSNR and SSIM.

Keywords*: Image restoration, Wavelet transform, Canny edge, GLCM, Rich edge region, Elastic net*

INTRODUCTION

Blind image deblurring aims to recover the blur kernel and sharp latent image from a blurred image [10]. When the blur is uniform, a blurred image is evaluated using Eqn (1).

$$I = L \otimes k + n \tag{1}$$

where I, L and k are the observed blurred image, latent clear image, and blur kernel respectively. n denotes the additive noise and $\otimes$ denotes the convolution operator. From the eqn 1 only blurred image I is known and many different pairs of L and k contribute to same I. The blind image restoration of a single image has significant practical and research value [16], [18]. However, due to the lack of information, single image restoration is a difficult task [14], [8].

 https://doi.org/10.37896/pd91.4/91451

ISSN: 0369-8963

Image deblurring algorithm for non-uniform motion blur images uses to propagate a uniform defocus map, removes the blurred parts partially where edges are not clear [4]. A novel scale-invariant image prior to an algorithm is applicable to different blurred models and has achieved successful results. However, several shortcomings still exist in the blur kernel estimation process [11].

An approach to remove motion blurring from a single image is by formulating the blind blurring model. The method removed the ambiguity between blur kernel and clear image but it is time-consuming [19]. An algorithm is based on a model-based motion estimation approach for monocular videos with explicit modeling of motion blur, achieves better deblurring. But more iterations occur to the motion and texture estimation loop and have high complexity in processing [20]. Adaptive anisotropic regularization and refinement of the blur kernels are incorporated into an iterative process to improve the precision of blur kernel [3]. However, the ringing effects were obvious and extensive computation is required.

A complete blind deblurring algorithm handles image motion blur with image edge prior [6], consumes more time than conventional deconvolution. The idea of using a piecewise function to the distribution of the natural image gradient shows visible distortion around the edges but suffers from staircase effect in the smooth area [8].

Blind motion deblurring method using prior image knowledge uses a mixed Gaussian model to the heavy tail distribution of natural image gradient and estimates the blur using the statistics of natural image [11]. However, the ringing effects were obvious and extensive computations were required. Deblurring text images via L_0-regularized intensity and gradient prior [21], uses prior knowledge of intensity and gradient. However, the restoration with prior knowledge is an iterative method and has a visually significant structure, such as large-scale edges and small-scale details [11].

Fast deblurring algorithm for blur kernel estimation process, has the retained gradient value greater than a threshold, and optimization function were established using image gradient. The algorithm's deblurring effect improved greatly; however, the recovery results were not always ideal, especially for images with rich details [1]. The nonlocal sparse regularization-based image deblurring technique [28] improves the accuracy of deblurring and achieves better peak signal-to-noise but does not consider the high dimensional information. Group sparsity-inducing regularize is based on image gradient on L_1 and L_2, local group

 https://doi.org/10.37896/pd91.4/91451

ISSN: 0369-8963

clustering provides better results but the blur kernel estimation process has too many iterations [31] and has artifacts along the edges.

A low rank prior to blind image deblurring [29] is difficult to model more complex structures of natural images only using adjacent image pixels, as natural images contain complex structures. The L_0-regularized intensity and gradient prior to text image deblurring use the half-quadratic splitting method. The splitting method guarantees that each sub-problem has a closed-form solution and ensures fast convergence. But it takes more time to calculate point spread function for convolution [22]. The distortion correction model uses an algebraic transformation to approximate the back-mapping expansion polynomial and a least squares estimation method to minimise computation complexity. However, computation is still necessary[33].

A combination of L_1 and L_2 regularization reduces over-blurring around edges [23]. The convergence rate of this algorithm is better than the other algorithm. Elastic-net regularization-based kernel estimation [24,30] provides strong convexity and helps to preserve major structures. However, existing deblurring methods usually fail when sharp edges are not available. The work on elastic net-based image deblurring offers a promising solution but it is hard to estimate kernel and sparsity [30]. The high-frequency layer extraction using bilinear interpolation in luminance channel, rich edge region index calculation using a sliding window and gray-level co-occurrence matrix (GLCM), blur kernel estimation using L_0-regularized intensity for gradient prior and blind restoration are the methods used for image deblurring [2]. In this method, the size of the rich edge region is fixed and the de-blurring results are not sufficient.

To overcome this, image deblurring using GLCM and elastic net regularization have been proposed in this paper. The proposed method has three major contributions. First, the high-frequency layer is extracted from the blurred image using a 2D Haar wavelet transform in the luminance channel value of the input blurred image. Second, the rich edge region is extracted from the high-frequency layer using a gray-level co-occurrence matrix and sliding window concepts after using the Canny edge detection. This rich edge region has more information on the blur kernel. Third, the extracted rich edge region estimates the blur kernel with elastic net regularization and the blurred image is blindly restored. This greatly reduces the recovery time.

The rest of the paper is organized as follows. Section 2, presents the proposed image deblurring algorithm. The experimental results and validation are discussed in Section 3. Finally, section 4 concludes this paper.

 https://doi.org/10.37896/pd91.4/91451

ISSN: 0369-8963

PROPOSED IMAGE DEBLURRING ALGORITHM

The proposed method is based on rich edge region extraction using GLCM [2], as shown in Figure 1. First, separate the luminance channel for the blurred image and apply the 2D Haar wavelet transformation to extract the high-frequency layer of the image. Subsequently, the high-frequency layer image is divided into regions based on a sliding window, and the rich edge region index of each region is calculated. Finally, the region with the richest edge information is extracted to estimate the blur kernel using the elastic net, and the blurred image is blindly restored.

High-frequency layer is extracted from the blurred image using 2D Haar wavelet transform in luminance channel (I_Y) value of the blurred input image [32].

$$I_Y = 0.299 \times R + 0.587 \times G + 0.114 \times B \quad (2)$$

where R, G, B is the color channel value, of the blurred image (I). $I_Y$transformed from RGB color space of size of N×N is performed using 2D Haar wavelet(H) due to orthogonal in nature [26] and, for high frequency detail preservation.

The wavelet subbands are computed by sampling the functions with an array of length 2^n is represented as $I_Y(x,y)H(n)$ and is given in eqn (3).

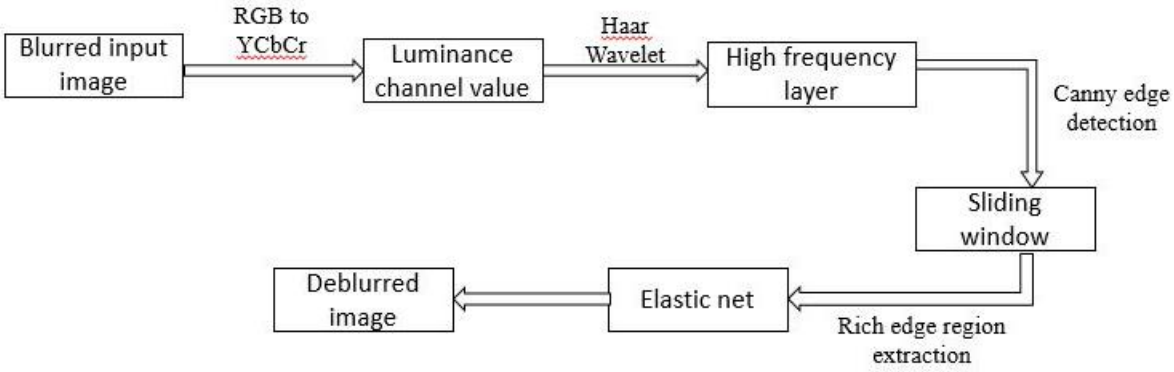

Fig:1

Block diagram of the proposed method

$$I_Y(x,y)H(n) = \begin{cases} I_Y H(n-1)[1,1] \\ 2^{\frac{n-1}{2}} I_Y K(n-1)[1,-1] \end{cases} \quad (3)$$

where K is the Kronecker product operation and (1,1) and (1, -1) are the unit interval of the Haar wavelet transform. The final Haar wavelet image $I_H(x,y)$is obtained by using eqn(4)

 https://doi.org/10.37896/pd91.4/91451

ISSN: 0369-8963

$$I_H(x,y) = I_Y H(n).I_Y H(n)^T \quad (4)$$

where $I_H$is the Haar wavelet image.

The high-frequency layer details from $I_H(x,y)$ is given to the canny edge detection algorithm to detect the wide range of edge with low error rate [25,30]. In canny edge detection initially, the gaussian operation is performed for $I_H(x,y)$ as given in eqn (5) to suppress the noise, undesirable details and texture. The hysteresis threshold $I_H(x,y)$is performed for the creation of a continuous edge map of the threshold image by removing the excessive edge pixels due to noise.

$$I_g = g_\sigma(x,y) * I_H(x,y) \quad (5)$$

where

$$g_\sigma = \frac{1}{\sqrt{2\pi\sigma^2}} \exp\left(-\frac{x^2+y^2}{2\sigma^2}\right) \quad (6)$$

where x, y are, σ is the standard deviation. The sobel gradient in horizontal $I_{g_x}(x,y)$ and vertical direction $I_{g_y}(x,y)$ value are computed using eqn (7) and (8) respectively. The gradient is computed for each pixel (x,y) by convolving the image with gradient masks.

$$I_{g_x}(x,y) = I_g(x+1,y) - I_g(x-1,y) \quad (7)$$

$$I_{g_y}(x,y) = I_g(x,y+1) - I_g(x,y-1) \quad (8)$$

The gradient magnitude and orientation of each pixel defines the strength and direction of the edge of each pixel respectively and is computed using eqn (9) and (10) respectively.

$$I_M(x,y) = \sqrt{I_{g_x}^2(x,y) + I_{g_y}^2(x,y)} \quad (9)$$

and

$$\theta(x,y) = \tan^{-1}\left[I_{g_y}(x,y) \,/\, I_{g_x}(x,y)\right] \quad (10)$$

The computed gradient image is applied for non-maxima suppression to convert the blurred edges in the image into sharp edges by preserving local maxima and suppressing minima. The potential edges are determined using low and high threshold values, based on potential edges of gradient magnitude histogram of the whole image is calculated. 20% of pixels in the image has been classified as strong edges based on the high threshold of gradient magnitude. 40% high threshold is considered a low threshold [30].

 https://doi.org/10.37896/pd91.4/91451

ISSN: 0369-8963

To further improve the edge detection, the edge details are performed with GLCM [2] for each 3×3 overlapping sliding window as shown in fig 2.

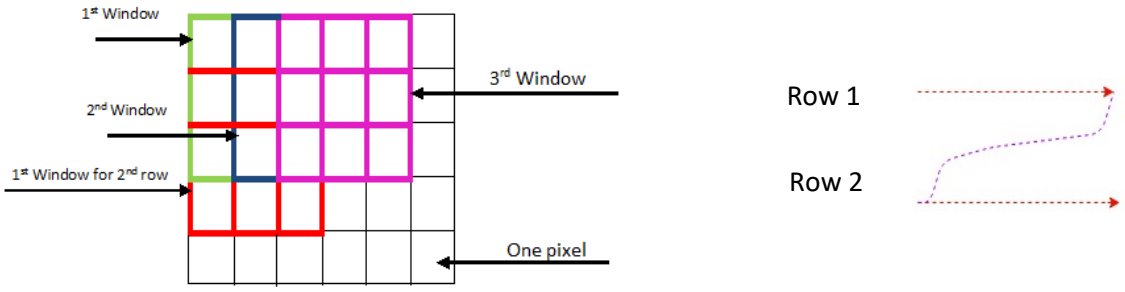

(a) (b)

Fig 2: Sliding window (a) operation (b) flow

Initially in GLCM, the sum of inertia and inverse difference moments are calculated at four different angles 0°,45°, 90°,and 135° as shown in fig 3. Fig 3a represents the direction of angle for the pixel of interest M. The angles (θ),0°, 45°, 90°, and 135° for both clockwise and anticlockwise directions for M is chosen as in fig 3b to find the contrast along with homogeneity.

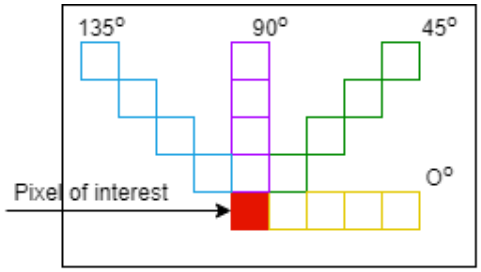

	M_{135}	M_{90}	M_{45}	
	M_0	M	M_0	
	M_{45}	M_{90}	M_{135}	

(a) (b)

Fig 3 GLCM pixel of interest (a)direction of angles(b) Sliding window angles

The moment of inertia (M_i) is the contrast ratio of the image to reveal the depth of image texture and, is computed using eqn (11)

$$M_i = M_i^0 + M_i^{45} + M_i^{95} + M_i^{135} \quad (11)$$

Inverse difference moment M_d from eqn (12) identifies the local homogeneity of the image.

https://doi.org/10.37896/pd91.4/91451

ISSN: 0369-8963

$$M_d = M_d^0 + M_d^{45} + M_d^{95} + M_d^{135} \quad (12)$$

where M_i^θ and M_d^θ are the moment of inertia and inverse difference moment respectively in the θ direction.

The rich edge region R_E is computed by subtracting the inverse difference moment from the moment of inertia as given in eqn (13).

$$R_E = M_i - M_d \quad (13)$$

The rich edge region index of each 3×3 window is computed using eqn (13) and the largest rich index I_{S_W} has been selected as a rich edge region from the blurred edge region [2] as given in eqn (14).

$$\begin{aligned} I_{S_W} &= Max(M_i - M_d) \\ &= Max\left(\Sigma\left(M_i^\theta(I_M)\right) - \Sigma\left(M_d^\theta(I_M)\right)\right) \\ &= Max\big(M_i(I_M) - M_d(I_M)\big) \\ &= Max\big(R_E(I_M)\big) \end{aligned} \quad (14)$$

The elastic net is applied to the rich edge region (I_{S_W}) to increase accuracy and sparsity. The elastic net includes L_1 and L_2 regularization as given in eqn (15).

$$\varphi\big(I_{S_W}\big) = \lambda_1 \sum_i \big\|I_{S_W}\big\|_\omega + \frac{\lambda_2}{2} \sum_i \big\|I_{S_W}\big\|_\omega \quad (15)$$

where $\lambda_1$and λ_2 are regularization parameters of L_1 and L_2 regularization, and ω is positive weights. Finally, the High resolution deblurred image (I_R) is computed using eqn (16).

$$I_R = \min_{I,k_1} \big\|I_{S_W} * k_1 - I\big\|_2^2 + \omega\varphi\big(I_{S_W}\big) \quad (16)$$

where I_{S_W} is the extracted rich edge region, I is the blur image of I_{S_W} in the blur kernel calculating process, k_1 is a blur kernel, ω is the weight of regularization, $\varphi\big(I_{S_W}\big)$ is the regularized term.

 https://doi.org/10.37896/pd91.4/91451

ISSN: 0369-8963

Steps for proposed deblurring algorithm

Input: Blurred input image $I(x,y)$ where x and y are the number of rows and columns

Output: Deblurred image $I_R(x,y)$

Step 1: Get the grayscale luminance value I_y from I.

Step 2: Apply 2D haar transformation on I_y and the resultant image is $I_H(x,y)$

Step 3: Perform a canny edge algorithm on $I_H(x,y)$

- [rows, columns] =size I_H
- Obtain the gradient I_{g_x} and I_{g_y}

for x=1 to rows

for y=1 to columns

$$I_{g_x}(x,y) = I_g(x+1,y) - I_g(x-1,y)$$

$$I_{g_y}(x,y) = I_g(x,y+1) - I_g(x,y-1)$$

end for

end for

- obtain the gradient magnitude $I_M(x,y)$.

Step 4: Apply GLCM for canny edge image for each 3×3 overlapping sliding window

- Obtain the image size (I_M), [rows, columns] =size ((I_M)
- Set (x,y) of the initial region, initial window start=0, and displacement of d_x and d_y=0
- GLCM matrix is [row, column]=G_{mat}

for x=0: rows

for y=0; columns

$x_1 = x + dx$ and $y_1 = y + dy$

$if\ ((x_1 \geq 0) and (y_1 \geq 0) and (x_1 < G_{mat}) and (y_1 < G_{mat}))$

$bin1 = I_H(x,y)\ /\ 256$

$bin2 = I_H(x_1,y_1)\ /\ 256$

GLCM $(bin1, bin2)$=GLCM $(bin1, bin2)$+1

count=count+1

end if

end for

end for

- Calculate the largest rich index using eqn(16)

Step 5: Apply the Elastic-net regularization to rich edge region, to find a deblurred image $I_R(x,y)$

https://doi.org/10.37896/pd91.4/91451

ISSN: 0369-8963

Experimental results and Discussion

This paper focuses the solution on non-uniform motion blur and unknown blur kernel problem caused by blur images. The proposed method has been simulated using MATLAB R2017b in a personal computer of 64-bit windows 10 with an Intel processor 3.4-GHz and 8 GB RAM. To show the effectiveness of the proposed method, the proposed algorithm has been compared with the existing image deblurring algorithms.

The task of image deblurring is very critical in computer vision to restore the real image and preserve as much important structures like edges and texture details without spurious distortion is still challenging. A low rank prior to blind image deblurring is more complex in natural images and obtains low accuracy during evaluation [29]. Non local sparse regularization L_0 [28] and L_0-regularized intensity for gradient prior [2] gives a competitive performance than motion tracking [20] but it provides less identification of kernel and sparsity. Group sparsity [31] based local group clustering provide better results but distortion occurs around the edges. The work on elastic net based image deblurring offers a promising solution but is hard to identify the sparsity [30]. Hence the existing methods [29], [20], [28], [30], [2], [31] and proposed methods are experimentally analyzed for image deblurring.

The proposed method uses a naturally blurred image from CERTH image dataset [27]. The CERTH image dataset consists of totally 2450 digital images, including 1219 undistorted images,631 naturally blurred images and 600 artificially blurred images. The proposed method is assessed by two objective image quality metrics, Peak Signal to Noise Ratio (PSNR) and Structural Similarity Index Metric (SSIM) and further been analyzed for visual quality on the restored image.

3.1 Deblurring evaluation of different methods for digital blur

The proposed deblurring method has been compared with existing deblurring methods to show the effectiveness of the deblurred image. Table 1 gives the PSNR and SSIM of existing and proposed deblurring method for various digital blur images of CERTH dataset. From table 1 it is observed that, the proposed method gives 16%,14%,11%,7%,5% and 2% high average PSNR compared to recently analyzed methods of Wenqi et al [29], Clemens et al[20], Wang et al [28], Hongyan et al[30], Minghua et al[2], and Dong et al [31] respectively due to high texture detail description and predictor correlation. Fig 4 shows the visual quality analysis of the proposed deblurred algorithm. From the zoom portion of the deblurred

 https://doi.org/10.37896/pd91.4/91451

ISSN: 0369-8963

image, it has been observed that the proposed deblurred image is clearer than the existing methods, as the elastic net is consistent in prediction and feature selection by removing staircase effect.

Table 1: Evaluation of deblurred image

S.no	Algorithms	Images									
		(i)		(ii)		(iii)		(iv)		(v)	
		PSNR	SSIM	PSNR	SSIM	PSNR	SSIM	PSNR	SSIM	PSNR	SSIM
1	Wenqi [29]	23.5987	0.6074	24.2154	0.7202	23.1548	0.7532	20.1124	0.8732	21.1023	0.7564
2	Clemens [20]	24.0125	0.6321	25.3146	0.7759	24.0356	0.7798	23.0157	0.8775	21.9654	0.7812
3	Wang [28]	25.0165	0.6281	26.0149	0.7612	24.8697	0.7921	23.0584	0.8798	22.0635	0.7915
4	Hongyan [30]	26.2154	0.6214	26.5489	0.7716	25.0124	0.8094	23.1547	0.8892	23.8452	0.8006
5	Minghua [2]	26.4857	0.7012	26.7892	0.7812	26.1862	0.8125	25.0263	0.8918	24.5294	0.8098
6	Dong[31]	27.5689	0.7124	26.9875	0.8189	27.0152	0.8245	24.0568	0.9006	25.1024	0.8114
7	Proposed	28.0065	0.7285	27.2923	0.8351	27.8947	0.8263	25.6541	0.9194	25.5806	0.8197

https://doi.org/10.37896/pd91.4/91451

ISSN: 0369-8963

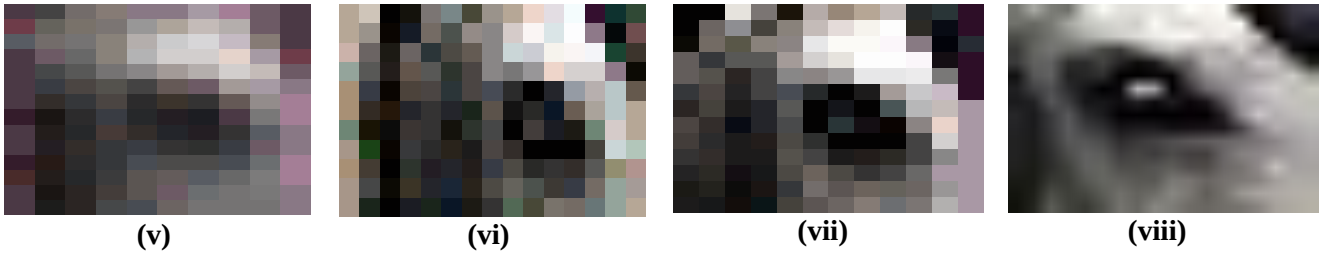

Fig 4: Sample deblurred images of CERTH dataset
(i)Blur image (ii) Wenqi [29] (iii) Clemens [20] (iv) Wang [28] (v) Hongyan [30] (vi) Minghua [2] (vii) Dong[31] (viii) Proposed

To evaluate the proposed method objectively, the average PSNR of the restored images of different methods has been compared and shown in fig 5. From fig 5, it has been observed that the PSNR of the proposed method is superior than other existing methods. The average PSNR and SSIM of the proposed method is improved by 6.01 dB [29], 4.64 dB [20], 3.41 dB [28], 2.13 dB [30],1.28 dB [2] and 0.93 dB [31]. 0.087 [29],0.063 [20],0.038 [28], 0.019 [30],0.009 [2], and 0.008 [31] respectively. This increase in average PSNR and SSIM is due to better identification of texture details information in recursive manner and use of high prediction elastic net.

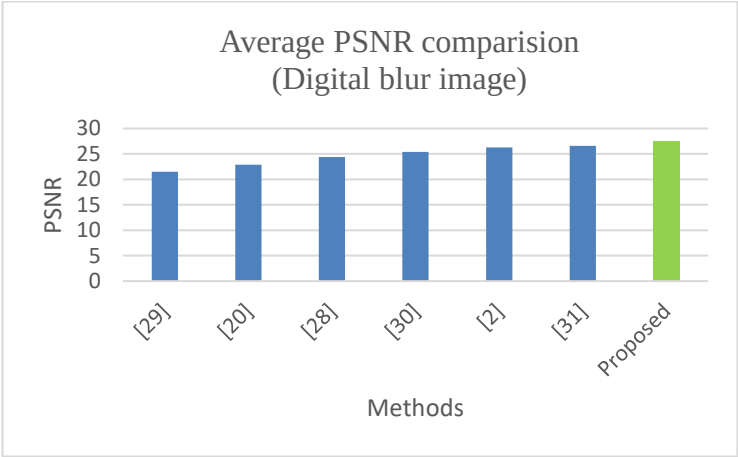

Fig 5: Image deblurring: Average PSNR comparison

3.2. Deblurring evaluation of different methods for naturally blurred images

The proposed method has been evaluated on the benchmark dataset CERTH 631 of naturally blurred images and is compared with existing deblurring methods Wenqi et al [29], Clemens et al [20], Wang et al [28], Hongyan et al [30], Minghua et al [2], and Dong et al [31]. Table 2 shows the comparison of PSNR

https://doi.org/10.37896/pd91.4/91451

ISSN: 0369-8963

and SSIM for the proposed and other deblurring methods. The PSNR and SSIM of the proposed method has been improved by 4.23 dB [29], 4.06 dB [20], 3.32 dB [28],2.86 dB[30], 1.75 dB[2] and 0.56 dB[31] and 0.075 [29] , 0.068[20], 0.041[28], 0.034[30],0.032[2] and 0.021[31] respectively.

For visual assessment, existing and proposed deblurred images of doll, and the corresponding zoom part obtained from the deblurred image are shown in Fig 6. In the smooth areas of the image in figure Fig. 6 (viii) the noises are removed perfectly, while in smooth areas of the other images in Fig.6, has annoying distortion. Fig 7 shows the comparison of average PSNR of the naturally deblurred images from CERTH database for the proposed and existing deblurring methods. The proposed deblurring method provides better deblurring than other methods due to well-measured luminance, edge description, texture details and more accurate prediction of blurred and deblurred images. In naturally blurred image dataset, the observed PSNR of the proposed method is better than other method due to edge details recovery and texture.

Table 2: Deblurring performance of naturally blurred image

S.no	Algorithms	Images									
		(i)		(ii)		(iii)		(iv)		(v)	
		PSNR	SSIM	PSNR	SSIM	PSNR	SSIM	PSNR	SSIM	PSNR	SSIM
1	Wenqi [29]	21.7837	0.6859	21.7713	0.7561	22.9515	0.7353	20.0367	0.8863	20.062	0.7478
2	Clemens [20]	23.8468	0.6998	24.7278	0.7628	23.5734	0.7716	20.1323	0.8972	21.1515	0.7717
3	Wang [28]	24.2606	0.7245	25.827	0.8185	24.4542	0.7982	23.0356	0.9015	22.0146	0.7965
4	Hongyan [30]	25.2646	0.7205	26.5273	0.8038	25.2883	0.8105	23.0783	0.9038	22.1127	0.8068
5	Minghua [2]	26.4635	0.7238	27.0613	0.8142	25.431	0.8278	23.1746	0.9132	23.8944	0.8159
6	Dong[31]	27.6645	0.8024	28.0152	0.8801	28.0254	0.8394	25.0196	0.9403	25.3256	0.8304
7	Proposed	28.2546	0.8209	27.8047	0.8777	28.3133	0.8447	25.674	0.9434	25.6298	0.835

https://doi.org/10.37896/pd91.4/91451

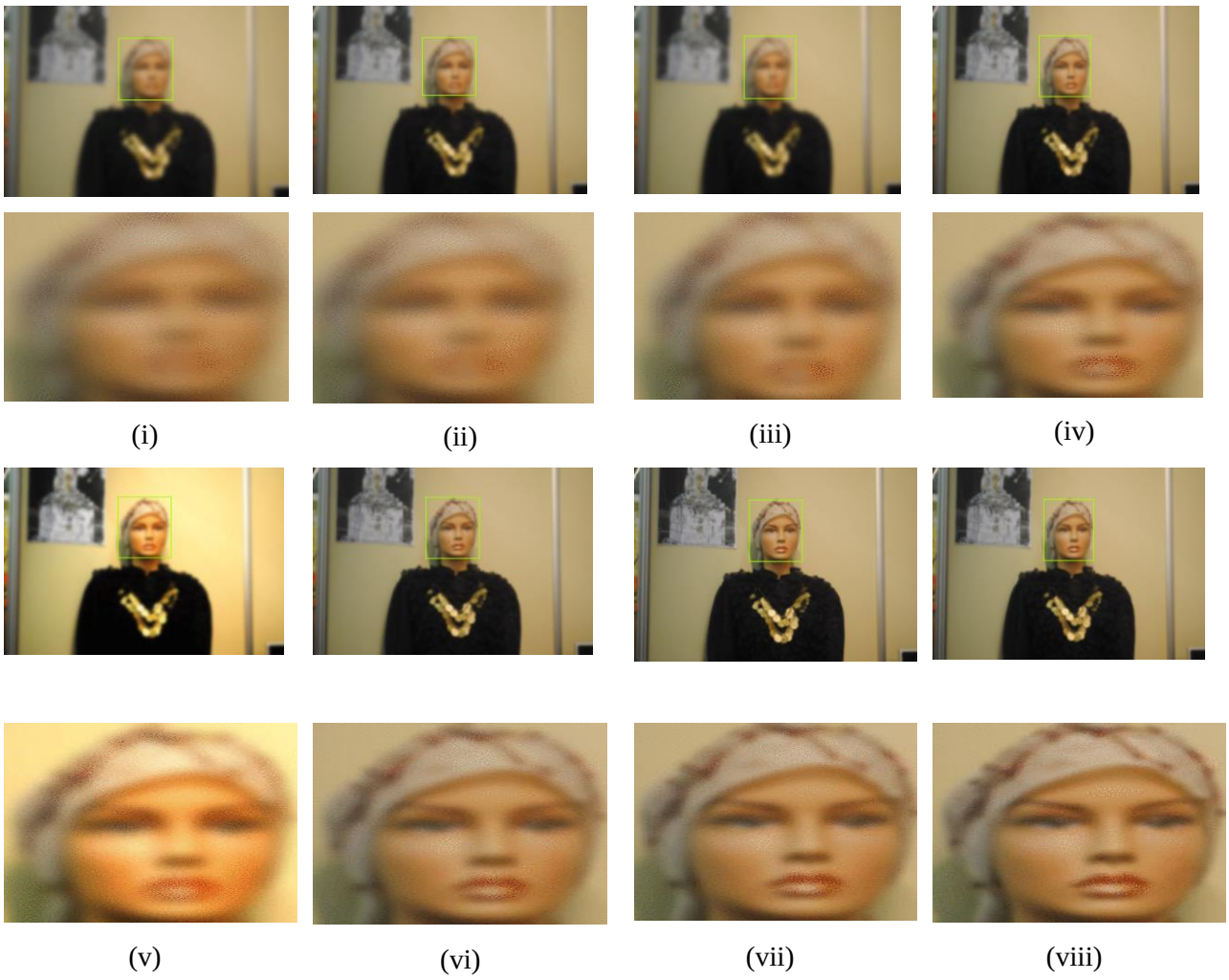

Fig 6: Synthesized from the ground truth dataset CERTH:Results comparison are deblurred by (i)Blur image (ii) Wenqi [29] (iii) Clemens [20] (iv) Wang [28] (v) Hongyan [30] (vi) Minghua [2] (vii) Dong[31] (viii) Proposed

 https://doi.org/10.37896/pd91.4/91451

ISSN: 0369-8963

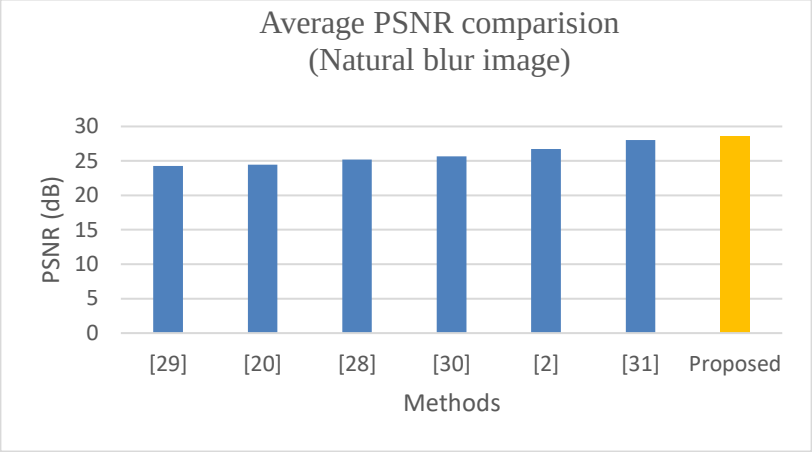

Fig 7: Natural blur dataset average PSNR comparison for various methods

3.3. Quantitative evaluation

The proposed method has been evaluated on the benchmark dataset CERTH. The error ratio metric [18] commonly used to evaluate the restored, is computed using eqn19

$$E_R = \|I - I_R\|_2^2 \quad (19)$$

where I, is the blurred image, I_R is the restored image obtained from the estimated blur kernel. Proposed method has been compared to existing deblurring methods [1-3,8,11,20,29]. Fig 8 shows the proposed and existing methods cumulative error ratio metric. The proposed method, has less error due to sharpness in edge regions, texture details and accurate prediction. The proposed method is outperforming than other existing methods.

https://doi.org/10.37896/pd91.4/91451

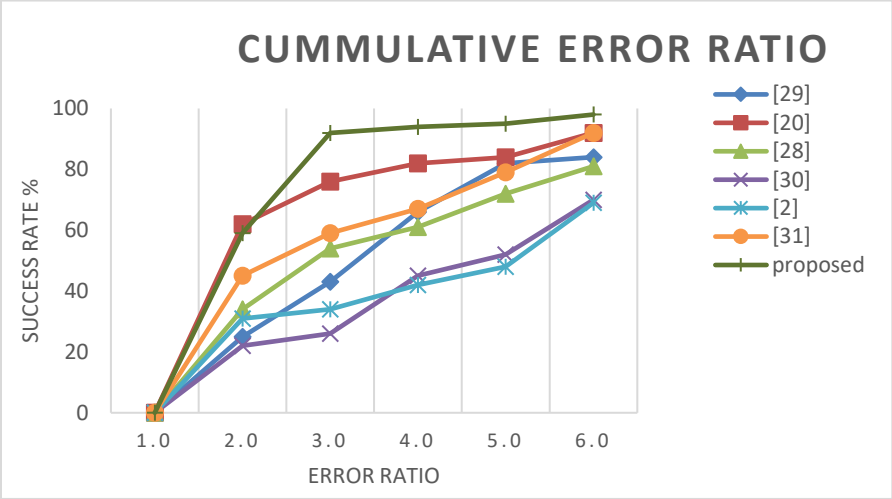

Fig 8: Cumulative error ratio

Conclusion and future scope

The proposed image deblurring method based on rich edge region extraction using a gray-level co-occurrence matrix has been designed and simulated. The proposed method based on DWT extracts high-frequency layer to perform canny and GLCM process. Further the blur kernel estimation process improves the edge information using elastic net and corrects the high-frequency components in image deblurring process. Experimental results shows that the proposed method achieves better performance than the existing methods in image deblurring. The proposed method not only effectively eliminates the motion blur of the image, but also improves the recovery efficiency to 7%. In future, this algorithm will be designed to automatically determine the size of the rich edge region and sliding interval of the sliding window with improved regularization method for better image restoration.

Conflict of Interest

The authors declare that they have no conflict of interest.

References

1. Cho. S., Lee.S., “Fast motion deblurring,”. ACM Trans Graph 28 (5),2009, 145.
2. Minghua.Z., Xin.Z., Zhenghao.S., Bing L.2018. Restoration of motion blurred images based on rich edge region extraction using a gray-level co-occurrence matrix. IEEE Trans. pp.15532-15540.

 https://doi.org/10.37896/pd91.4/91451

ISSN: 0369-8963

3. Hanyu H., Kyu Park., 2010. Single-image motion deblurring using adaptive anisotropic regularization. Spie Trans optical engineering, pp 097008(1-13).
4. Chia-Feng Chang, Jiunn-Lin Wu, and Ting-Yu Tsai.,2017. A Single Image Deblurring Algorithm for Nonuniform Motion Blur Using Uniform Defocus Map Estimation. Hindawi Mathematical Problems in Engineering. Pp 1-14.
5. Sun, L., Cho, S., Wang, J., Hays, J., 2013. Edge-based blur kernel estimation using patch priors. ICCP. pp. 1–8.
6. Jing W, Ke L, Qian W, Jie J.,2012. Kernel Optimization for Blind Motion Deblurring with Image Edge Prior. Hindawi Mathematical Problems in Engineering.
7. L. Zhong, S. Cho, D. Metaxas, S. Paris, and J. Wang,2013‘‘Handling noise in single image deblurring using directional filters,’’ in Proc. IEEE Conf. Comput. Vis. Pattern Recognit., pp. 612–619.
8. Shan, Q., Jia, J., Agarwala, A., 2008. High-quality motion deblurring from a single image. ACM Trans. Graph. 27 (3), 73.
9. Yanyang, Y., Wenqi, R., Yuanfang, G.,2017. Image Deblurring via Extreme Channels Prior. IEEE Conference on CVPR. pp. 4003-4011.
10. Krishnan, D., Tay, T., Fergus, R., 2011. Blind deconvolution using a normalized sparsity measure. IEEE Conference on CVPR. pp. 233–240.
11. Fergus, R., Singh B, Hertzmann A., Roweis S. T., Freeman W. T., 2006. Removing camera shake from a single photograph," ACM Trans. Graph., vol. 25, no. 3, pp. 787_794.
12. Levin, A., Weiss, Y., Durand, F., Freeman, W.T., 2011. Efficient marginal likelihood optimization blind deconvolution. IEEE Conference on CVPR. pp. 2657–2664.
13. Gupta,A., Joshi,N., Zitnick,C., Cohen,M., Curless,B., 2010. Single image deblurring using motion density functions. in Proc. Eur. Conf. Comput. Vis., vol. 6311. pp. 171_184.
14. Xu, L., Zheng, S., Jia, J., 2013. Unnatural l_0 sparse representation for natural image deblurring.CVPR. pp. 1107–1114.
15. Levin, A., Weiss,Y., Durand,F., Freeman.W.T.,2011. Understandingblind deconvolution algorithms. IEEE Trans. Pattern Anal. Mach. Intell.,vol. 33, no. 12, pp. 2354_2367,
16. Michaeli, T., Irani, M., 2014. Blind deblurring using internal patch recurrence. ECCV. pp.783–798.

 https://doi.org/10.37896/pd91.4/91451

ISSN: 0369-8963

17. Levin, A., Weiss, Y., Durand, F., Freeman, W.T., 2009. Understanding and evaluating blind deconvolution algorithms. IEEE Conference on CVPR. pp. 1964–1971.
18. Haiqian,Y and Miriam, L., 2005. Optimizing Data Intensive Window-based Image Processing on Reconfigurable Hardware Boards. IEEE Workshop on Signal Processing Systems.
19. Cai,J.F., Ji,H., Liu,C., Shen,Z., 2009. Blind motion deblurring from a single image using sparse approximation. in Proc. IEEE Conf. Comput.Vis. Pattern Recognit., pp. 104_111.
20. Clemens,S., Anna, H., Peter Eiserta, b., 2017. Model-Based Motion Blur Estimation for the Improvement of Motion Tracking. Elsevier Trans on Computer Vision and Image Understanding.
21. Pan J, Hu Z, Su Z, Yang M.H., 2014. Deblurring text images via L0-regularized intensity and gradient prior. in Proc. IEEE Conf. Comput. Vis.Pattern Recognit., pp. 2901_2908.
22. Jinshan P, Hu Z, Su Z, Yang M. 2014. Deblurring Text Images via L0-Regularized Intensity and Gradient Prior. IEEE Conference on CVPR. pp. 2901-2908.
23. Kemal O, Seke E, 2011. Combination of l_1 and l_2 Norms for Image Deconvolution Problems. 7th International Conference on Electrical and Electronics Engineering.
24. Kim E, Lee M, Oh S. 2015. Elastic net regularization of singular values for robust subspace learning. IEEE Conference on CVPR. pp. 2901-2908.
25. Yu H, Lee M ., 2005, Optimizing Data Intensive Window-based Image Processing on Reconfigurable Hardware Boards", IEEE Workshop on Signal Processing Systems.
26. Yi Z, Keigo H, 2013. Blur Processing Using Double Discrete Wavelet Transform. CVPR. pp. 1091–1098.
27. E. Mavridaki, V. Mezaris, No-Reference blur assessment in natural images using Fourier transform and spatial pyramids, Proc. IEEE International Conference on Image Processing (ICIP 2014), Paris, France, October 2014.
28. Nannan Wang, Wenxuan Shi, Ci’en Fan, and Lian Zou. 2018. An improved nonlocal sparse regularization-based image deblurring via novel similarity criteria, International Journal of Advanced Robotic Systems.
29. Wenqi Ren, Xiaochun Cao, Jinshan Pan, Xiaojie Guo, Image Deblurring via Enhanced Low-Rank Prior, ieee transactions on image processing, vol. 25, no. 7, July 2016.

 https://doi.org/10.37896/pd91.4/91451

ISSN: 0369-8963

30. Hongyan wang, Jinshan Pan, Zhixun Su, Songxin Liang, (2018), Blind image deblurring using elastic-net based rank prior, Elsevier transaction on computer vision and image understanding 168, page no 157-171.
31. Dong Gong, Rui Li, Yu Zhu, Haisen Li, Jinqiu Sun, Yanning Zhang, (2018), Blind image deblurring by promoting group sparsity, Elsevier transaction on Neurocomputing, page no 1-11.
32. Jaime A. Martins, Joao M. F. Rodrigues, Hans du Buf, Luminance, Colour, Viewpoint and Border Enhanced Disparity Energy Model, Transaction on Plos , page no 1-24.
33. Mylsamy, Mohankumar & Gopalakrishnan, V. & Mohankumar, s.Yasotha. (2015). A vlsi approach for distortion correction in surveillance camera images. ARPN Journal of Engineering and Applied Sciences. 10. 4105-4108.

 https://doi.org/10.37896/pd91.4/91451